Research Square

Preprints are preliminary reports that have not undergone peer review.
They should not be considered conclusive, used to inform clinical practice,
or referenced by the media as validated information.

Integrated Multi-Omics Analysis Identifies ATAD5 as a Mediator of Tumor Plasticity and Immunosuppressive Microenvironmental Remodeling in Castration-Resistant Prostate Cancer

Ruitao Li
Department of Urology, Tianjin Institute of Urology, The Second Hospital of Tianjin Medical University
Yi Zheng
Department of Urology, Tianjin Institute of Urology, The Second Hospital of Tianjin Medical University
Junlin Shen
Department of Urology, Tianjin Institute of Urology, The Second Hospital of Tianjin Medical University
Hongli Zhang
Department of Urology, Tianjin Institute of Urology, The Second Hospital of Tianjin Medical University
Cheng Fang
Department of Urology, Tianjin Institute of Urology, The Second Hospital of Tianjin Medical University
Xiepeng Zuo
Department of Urology, Tianjin Institute of Urology, The Second Hospital of Tianjin Medical University
Zhen Zhou
Department of Urology and Guangdong Key Laboratory of Urology, First Affiliated Hospital of Guangzhou Medical University
Pu Wang
Department of Urology, Henan Provincial People's Hospital
Jianpeng Yu
yujianpeng@tmu.edu.cn
Department of Urology, Tianjin Institute of Urology, The Second Hospital of Tianjin Medical University
Yuanjie Niu
Department of Urology, Tianjin Institute of Urology, The Second Hospital of Tianjin Medical University

Research Article

Keywords: ATAD5, castration-resistant prostate cancer, tumor stemness, tumor microenvironment, single-cell RNA sequencing, spatial transcriptomics, biomarker

Posted Date: October 16th, 2026

DOI: https://doi.org/10.21203/rs.3.rs-11146748/v1

License: This work is licensed under a Creative Commons Attribution 4.0 International License.
Read Full License

Additional Declarations: No competing interests reported.

Abstract

Purpose

Castration-resistant prostate cancer (CRPC) is a lethal malignancy with limited therapeutic options. This study aimed to identify clinically relevant molecular markers linking tumor plasticity and microenvironmental remodeling in CRPC through integrated multi-omics analysis.

Methods

Transcriptomic data from three GEO cohorts (GSE32269, GSE35988, GSE80609; 68 CRPC, 87 LPCa) were analyzed by differential expression analysis and weighted gene co-expression network analysis (WGCNA). Hub genes were prioritized by stemness-like (SCL) association scoring and validated across TCGA-PRAD, SU2C/PCF, DKFZ, and ICGC cohorts. Immune infiltration was estimated using xCell. Single-cell RNA-seq (GSE137829) and spatial transcriptomics (GSE308486) resolved cellular and tissue-level expression patterns. Immunohistochemistry (IHC) was performed on 10 LPCa and 10 CRPC specimens, and ATAD5 function was assessed by siRNA knockdown in C4-2 and 22Rv1 cells via Transwell invasion and colony formation assays.

Results

WGCNA identified the MEblack module as most strongly correlated with CRPC status ($r = 0.72$), enriched in stemness and DNA replication programs. ATAD5 ranked highest by SCL score (0.89) among hub genes. High ATAD5 expression consistently associated with shorter OS, PFS, DSS, and relapse-free survival across all four independent cohorts, and with advanced T stage, nodal involvement, higher Gleason score, and elevated PSA. ATAD5-high tumors exhibited reduced cytotoxic T-cell signatures, increased cancer-associated fibroblast enrichment, and upregulation of immune checkpoint genes (IDO1, CTLA4, CD274, LAG3, TIGIT). Single-cell analysis revealed ATAD5 predominantly in malignant epithelial cells with higher SCL scores, late pseudotime enrichment, and stronger predicted interactions with CAFs and myeloid cells. IHC confirmed elevated ATAD5, CD44, FAP, and CD8A protein in CRPC. ATAD5 knockdown significantly reduced invasion and colony formation in both cell lines ($p < 0.05$).

Conclusion

ATAD5 marks an aggressive, plasticity-associated malignant epithelial state in CRPC, linked to immunosuppressive microenvironmental features and adverse clinical outcomes, warranting further investigation of its therapeutic potential.

Introduction

Prostate cancer is one of the most commonly diagnosed malignancies in worldwide [1, 2, 3]. Although androgen deprivation therapy, androgen receptor-targeted agents, taxane-based chemotherapy, and poly(ADP-ribose) polymerase inhibitors have improved treatment options, many patients eventually develop castration-resistant prostate cancer (CRPC), which remains largely incurable [4, 5, 6, 7, 8]. CRPC is driven by diverse mechanisms, including androgen receptor amplification, activating mutations, splice variants such as AR-V7, and the emergence of androgen receptor-low or neuroendocrine states [9, 10, 11, 12, 13, 14, 15]. These features contribute to substantial molecular heterogeneity and therapeutic resistance.

Tumor cell plasticity is an important feature of CRPC progression. Under therapeutic pressure, prostate cancer cells may acquire transcriptional programs associated with stemness, self-renewal, invasion, and treatment resistance [16, 17, 18, 19, 20, 21, 22, 23]. Epigenetic reprogramming, Wnt/β-catenin signaling, Hippo pathway dysregulation, and altered nuclear receptor activity have all been implicated in the development of plastic malignant cell states [17, 18, 19, 24, 25, 26, 27, 28, 29, 30]. However, the molecular markers that identify aggressive and plastic malignant epithelial populations in CRPC remain incompletely defined.

The tumor microenvironment also contributes to CRPC progression and treatment resistance. Cancer-associated fibroblasts, tumor-associated myeloid cells, and dysfunctional T cells can promote stromal remodeling, immune exclusion, and impaired antitumor activity [31, 32, 33, 34, 39, 40, 41]. The expression of immune checkpoint molecules, including CD274, CTLA4, LAG3, and TIGIT, further reflects the immunosuppressive characteristics of advanced prostate cancer [35, 36, 37, 38]. However, the relationship between tumor-intrinsic plasticity-associated programs and microenvironmental features in CRPC remains poorly understood.

ATPase family AAA domain-containing protein 5 (ATAD5) is involved in DNA replication fidelity and genome maintenance. It participates in PCNA unloading from chromatin and contributes to DNA damage responses through interactions with proteins involved in DNA repair [42, 43]. Rare ATAD5 variants have also been reported in patients with breast and ovarian cancer [44]. Nevertheless, the expression pattern, clinical relevance, cellular distribution, and functional significance of ATAD5 in CRPC have not been systematically investigated.

In the present study, we integrated bulk transcriptomic, single-cell, spatial transcriptomic, clinical, tissue-level, and functional data to characterize ATAD5 in CRPC. We first identified CRPC-associated co-expression programs using transcriptomic datasets from three independent GEO cohorts. We then evaluated the associations of ATAD5 with clinical outcomes, clinicopathological features, immune and stromal signatures, and malignant epithelial cell states. Single-cell and spatial transcriptomic analyses were used to contextualize ATAD5 expression across cellular and tissue compartments, while immunohistochemistry provided protein-level validation. Finally, the effects of ATAD5 depletion on invasion and colony formation were examined in CRPC cell models. This study identifies ATAD5 as a

candidate marker of a plastic malignant epithelial state associated with aggressive CRPC biology and provides a basis for further investigation of its causal and therapeutic significance.

Materials and Methods

Public Dataset Acquisition and Preprocessing

Three publicly available RNA-seq datasets were retrieved from the Gene Expression Omnibus (GEO) database (https://www.ncbi.nlm.nih.gov/geo) as the discovery cohort: GSE32269, GSE35988, and GSE80609, comprising 68 castration-resistant prostate cancer (CRPC) and 87 localized prostate cancer (LPCa) samples. Raw count matrices were downloaded and normalized using variance-stabilizing transformation (VST) as implemented in the DESeq2 package (version 1.46.0) in R (version 4.4.3). Normalized expression values were subsequently $\log_2$-transformed and quantile-normalized across datasets. The three preprocessed matrices were merged by intersecting common gene symbols. Batch effects arising from differences in sequencing platforms and sample processing were removed using the harmony package (version 1.2.1). The efficacy of batch correction was confirmed by principal component analysis (PCA), with samples clustering by disease status rather than dataset of origin following correction. For independent validation, two additional cohorts were employed: The Cancer Genome Atlas Prostate Adenocarcinoma (TCGA-PRAD) dataset, accessed via the TCGAbiolinks package (version 2.34.0), and the SU2C/PCF International Prostate Cancer Dream Team dataset, obtained from cBioPortal (https://www.cbioportal.org). These cohorts were processed independently using the same normalization pipeline described above and were not included in batch correction or WGCNA analyses.

Differential expression analysis between CRPC and LPCa samples was performed on the integrated discovery cohort using the limma package (version 3.62.1). A linear model was fitted to the merged expression matrix using the lmFit function, followed by empirical Bayes moderation via eBayes. Differentially expressed genes (DEGs) were extracted using topTable and filtered by $|\log2FC| > 1$ and $P < 0.05$. Results were visualized as volcano plots and heatmaps using the ggplot2 (version 3.5.1) and ComplexHeatmap (version 2.22.0) packages, respectively. Gene Set Enrichment Analysis (GSEA) was conducted on the full ranked gene list using the clusterProfiler package (version 4.14.3) against Hallmark and KEGG gene sets from MSigDB (version 2024.1.Hs), with 1,000 permutations and a minimum gene set size of 15. Gene sets with $P < 0.05$ and $|NES|>1.0$ were considered significantly enriched.

Weighted Gene Co-expression Network Analysis (WGCNA)

To identify co-expression modules associated with CRPC progression, Weighted Gene Co-expression Network Analysis (WGCNA) was performed on the integrated discovery cohort using the WGCNA package (version 1.73) in R (version 4.4.3). Prior to network construction, genes with low expression variance were filtered by retaining the top 25% most variable genes across all samples, based on median

absolute deviation (MAD). A signed hybrid network was constructed using the blockwiseModules function. The soft-thresholding power was determined by the scale-free topology criterion, selecting the lowest power at which the scale-free topology model fit index exceeded 0.85 while maintaining reasonable mean connectivity; a soft-thresholding power of 4 was selected accordingly. Additional network parameters were set as follows: minimum module size of 30 genes, merge cut height of 0.25, and a TOMType of “signed”. Modules were identified using dynamic tree cutting and subsequently merged if their eigengene correlation exceeded 0.75. Module-trait correlations were computed by correlating each module eigengene (ME) with the binary disease status variable (CRPC = 1, LPCa = 0) using Pearson correlation, with significance assessed by Student’s t-test. Hub genes within the trait-associated module of interest were defined by two criteria applied simultaneously: module membership (MM) > 0.7 and gene significance (GS) > 0.4. GSEA was subsequently applied to genes within the module of interest, ranked by MM, to characterize the biological processes enriched within the module, using the same parameters described in Section 2.2.

Survival Analysis and Prognostic Validation

The prognostic value of ATAD5 was evaluated across four independent cohorts. Patients were stratified into high and low expression groups by median ATAD5 expression. Kaplan–Meier survival curves were compared using the log-rank test, with the following endpoints applied per cohort: DFS and PFS in TCGA-PRAD; OS in SU2C/PCF; relapse-free time in DKFZ; and OS in ICGC. All analyses were performed using the survival (version 3.7.0) and survminer (version 0.4.9) packages in R (version 4.4.3).

Immune Infiltration Analysis

Immune cell infiltration was estimated using the xCell algorithm implemented in the Immunedeconv package (version 2.1.0). Samples were stratified by median ATAD5 expression, and differences in immune cell enrichment scores between ATAD5-high and ATAD5-low groups were assessed using the Wilcoxon rank-sum test. Spearman correlation was applied to evaluate the association between ATAD5 expression and individual immune cell scores. All analyses were performed in R (version 4.4.3).

Single-Cell RNA Sequencing Analysis

Single-cell RNA sequencing (scRNA-seq) data were obtained from the GEO database (GSE137829) and processed using the Seurat package (version 5.2.0) in R (version 4.4.3). Quality control was performed by retaining cells with detected gene counts between 200 and 5,000, UMI counts exceeding 500, and mitochondrial gene fraction below 20%. Doublets were removed using the DoubletFinder package (version 2.0.4). Data were normalized using NormalizeData, and the top 2,000 highly variable genes were identified via FindVariableFeatures. After PCA on scaled data, batch effects were corrected using Harmony (version 1.2.1). Clustering was performed using FindNeighbor and FindClusters, and cells were visualized by UMAP and tSNE. Cell type annotation was performed manually based on canonical marker

gene expression. To distinguish malignant from normal epithelial cells, copy number variation (CNV) was inferred using inferCNV (version 1.22.0), with T cells and B cells serving as the copy-number–neutral reference population. Cells were classified as malignant epithelial if CNV score (mean absolute deviation from reference) > 0.01 and CNV correlation < 0.1; remaining epithelial cells were retained as normal epithelial. Cell–cell communication was analyzed using the CellChat package (version 2.2.0) with the built-in human ligand–receptor database. Interaction probabilities were computed using default parameters, and significant interactions were identified by permutation-based testing ($P < 0.05$).

Spatial Transcriptomic Analysis

Spatial transcriptomic data were retrieved from the Gene Expression Omnibus (GEO) under accession number GSE308486. This dataset comprised six prostate tissue sections, including three cases of prostatic ductal adenocarcinoma (PDA) and three non-PDA prostate cancer tissues (non-PDA). Sequencing was performed on the Illumina NovaSeq 6000 platform. Raw spatial expression matrices and corresponding tissue images were processed using the Seurat package in R. Spots with fewer than 200 detected genes or greater than 20% mitochondrial gene content were excluded from downstream analysis. Data normalization was performed using the SCTransform method. Dimensionality reduction, clustering, and cell type deconvolution were carried out to characterize the spatial distribution of epithelial, fibroblast, myeloid, and T cell populations across tissue sections. The spatial expression patterns of ATAD5, CD44, fibroblast activation protein (FAP), and CD8A were visualized using the SpatialFeaturePlot function. Given the limited sample size of three patients per group, spatial results were treated as exploratory and interpreted accordingly. All spatial transcriptomic analyses were performed in R (4.4.3).

Western Blotting

Western Blotting

Protein expression was assessed by western blotting. Cells were lysed in RIPA buffer (Beyotime, Shanghai, China) supplemented with protease inhibitor cocktail (Beyotime, Shanghai, China) on ice for 30 minutes. Lysates were centrifuged at 12,000 × g for 15 minutes at 4°C, and supernatants were collected. Protein concentrations were quantified using the BCA Protein Assay Kit (Solarbio, Beijing, China). Equal amounts of total protein (25 μg per lane) were resolved by sodium dodecyl sulfate–polyacrylamide gel electrophoresis (SDS-PAGE) on 8% polyacrylamide gels and subsequently transferred onto polyvinylidene fluoride (PVDF) membranes (Millipore, Burlington, MA, USA). Membranes were blocked with 5% non-fat dried milk in Tris-buffered saline containing 0.1% Tween-20 (TBST) for 1 hour at room temperature. Membranes were then incubated overnight at 4°C with the following primary antibodies: rabbit anti-ATAD5 (catalog no. 24954-1-AP; Proteintech, Wuhan, China; dilution 1:1000) and mouse anti-GAPDH (catalog no. 60004-1-Ig; Proteintech, Wuhan, China; dilution 1:10000). After three washes with TBST (10 minutes each), membranes were incubated with the appropriate horseradish

peroxidase (HRP)-conjugated secondary antibodies for 1 hour at room temperature. Protein bands were visualized using an enhanced chemiluminescence (ECL) detection reagent (Beyotime, Shanghai, China).

Immunohistochemistry (IHC)

Immunohistochemical staining was performed on formalin-fixed, paraffin-embedded (FFPE) tissue sections obtained from 10 patients with localized prostate cancer and 10 patients with castration-resistant prostate cancer (CRPC). Tissue sections were cut at 5 μm thickness, deparaffinized in xylene, and rehydrated through a graded ethanol series. Antigen retrieval was performed by heating sections in citrate buffer (pH 6.0) using a pressure cooker. Endogenous peroxidase activity was quenched by incubation with 3% hydrogen peroxide for 10 minutes at room temperature. Sections were blocked with normal goat serum for 30 minutes at room temperature to reduce non-specific binding. Sections were then incubated overnight at 4°C with the following primary antibodies: rabbit anti-ATAD5 (catalog no. bs-7656R; Bioss, Beijing, China; dilution 1:100), rabbit anti-CD44 (catalog no. 15675-1-AP; Proteintech, Wuhan, China; dilution 1:200), rabbit anti-FAP (catalog no. 11779-1-AP; Proteintech, Wuhan, China; dilution 1:100), and mouse anti-CD8A (catalog no. 66868-1-Ig; Proteintech, Wuhan, China; dilution 1:200). After three washes with phosphate-buffered saline (PBS), sections were incubated with the corresponding secondary antibodies using a horseradish peroxidase-conjugated IHC detection kit (catalog no. SP-9000; ZSGB-BIO, Beijing, China) according to the manufacturer's instructions. Signal was developed using 3,3'-diaminobenzidine (DAB) substrate, and sections were counterstained with hematoxylin, dehydrated, and mounted. All staining was evaluated independently by two pathologists who were blinded to patient clinical information. Positive staining area was quantified using ImageJ software (National Institutes of Health, Bethesda, MD, USA) and expressed as the percentage of positively stained area relative to the total tissue area. Statistical comparisons between the localized prostate cancer and CRPC groups were performed using the Mann–Whitney U test.

Cell Culture and siRNA Transfection

Prostate cancer cell lines were used in this study, including LNCaP, LNCaP-AI, C4-2, DU145, 22Rv1, and PC3. All cell lines were maintained in RPMI-1640 medium (Gibco, USA) supplemented with 5% fetal bovine serum (FBS; Gibco, USA) and 1% penicillin-streptomycin at 37°C in a humidified atmosphere containing 5% CO_2, with the exception of LNCaP-AI cells, which were cultured in RPMI-1640 supplemented with 5% charcoal-stripped serum (CSS; Gibco, USA) to simulate androgen-deprived conditions. All cell lines were routinely tested for mycoplasma contamination. For gene silencing, three small interfering RNAs (siRNAs) targeting human ATAD5 (Gene ID: 79915) were designed and synthesized by Beijing Saiotake Biotechnology Co Ltd. (Beijing, China) and dissolved in RNase-free water to a stock concentration of 100 μM. A non-targeting siRNA sequence was used as a negative control (siNC). The siRNA sequences used in this study are listed in Table 1. Cells were seeded in six-well plates at a density of 2×10^5 cells per well and allowed to adhere overnight. Transfection was performed using Lipofectamine 3000 reagent (Thermo Fisher Scientific, USA) according to the manufacturer's

instructions. siRNA was transfected at a final concentration of 50 nM. Cells were harvested 72 hours post-transfection for subsequent experiments.

Table 1
siRNA sequences used in this study

Name	Sense sequence (5'→3')	Antisense sequence (5'→3')
siRNA-1	5'-UCAAUUGUUGCCAAUUGAATT-3'	5'-UUCAAUUGGCAACAAUUGATT-3'
siRNA-2	5'-UUGCUUCUUGCUUGCUUGCTT-3'	5'-AGCAAGCAAGCAAGAAGCATT-3'
siRNA-3	5'-UUGAAGAAGAAGAAGAAGATT-3'	5'-UCUUCUUCUUCUUCUUCAATT-3'

Transwell Invasion Assay and Colony Formation Assay

Cell invasive capacity and clonogenic ability were assessed in C4-2 and 22Rv1 cells following ATAD5 knockdown with siRNA-3. For the Transwell invasion assay, cells were harvested 48 hours post-transfection, resuspended in serum-free RPMI-1640 medium, and seeded into the upper chamber of Transwell inserts (8 μm pore size; Corning, NY, USA) at a density of 5×10^4 cells per well. The lower chamber was filled with RPMI-1640 supplemented with 5% FBS as a chemoattractant. After 24 hours of incubation at 37°C, non-invaded cells on the upper surface were removed with a cotton swab, and invaded cells on the lower surface were fixed with 4% paraformaldehyde and stained with 0.1% crystal violet. Invaded cell numbers were quantified using ImageJ software (National Institutes of Health, Bethesda, MD, USA). For the colony formation assay, transfected cells were seeded in six-well plates at a density of 500 cells per well and cultured for 14 days. Colonies were fixed with 4% paraformaldehyde, stained with 0.1% crystal violet, and counted using ImageJ software. All experiments were performed in triplicate.

Results

Integrated Transcriptomic Analysis Identifies a CRPC-Associated Co-expression Program Linked to Malignant Cell Plasticity

To identify transcriptional programs underlying CRPC progression, we integrated RNA-seq data from three GEO cohorts comprising 68 CRPC and 87 LPCa samples. Following batch correction, PCA demonstrated clear separation of CRPC from LPCa along the first principal component (Fig. 1A). Differential expression analysis identified widespread transcriptomic alterations between the two groups, with upregulated genes in CRPC enriched in cell cycle and DNA replication processes (Fig. 1B–C). WGCNA identified multiple co-expression modules, among which the MEblack module showed the strongest positive correlation with CRPC status ($r = 0.72$; Fig. 1D–F). GSEA of MEblack module genes revealed significant enrichment in stemness-related programs, including RAMALHO_STEMNESS_UP (NES = 2.74, FDR $q < 0.01$) and

GOBP_POSITIVE_REGULATION_OF_STEM_CELL_POPULATION_MAINTENANCE (NES = 1.94, FDR q < 0.01), establishing this module as a CRPC-associated stemness transcriptional program (Fig. 1G).

The MEblack Module Is Associated with Adverse Outcomes and Immunosuppressive Microenvironmental Features

Patients stratified by MEblack eigengene score showed significantly worse PFS in the TCGA-PRAD cohort (HR = 2.569, 95% CI:1.723–3.890, $p = 1.22 \times 10^{-5}$) and OS (HR = 2.372, 95%CI:1.002–5.613, $p = 7.23 \times 10^{-3}$) in the SU2C/PCF cohort (Fig. 2A–B). Immune infiltration analysis using xCell revealed that ATAD5-high tumors had elevated stromal and microenvironment scores, reduced cytotoxic T cell populations, and increased CAF and endothelial cell infiltration (Fig. 2C). Immune checkpoint analysis further demonstrated upregulation of multiple inhibitory molecules including IDO1, CTLA4, CD274, LAG3, and TIGIT in ATAD5-high tumors, consistent with an immunosuppressive phenotype (Fig. 2D).

(A) Kaplan–Meier curve for progression-free survival (PFS) stratified by MEblack eigengene score in the TCGA-PRAD cohort (log-rank $p = 1.22 \times 10^{-5}$; HR = 2.569, 95% CI: 1.723–3.890). (B) Kaplan–Meier curve for overall survival (OS) stratified by MEblack eigengene score in the SU2C/PCF cohort (log-rank $p = 7.23 \times 10^{-3}$; HR = 2.372, 95% CI: 1.002–5.613). (C)Heatmap of xCell immune infiltration scores across ATAD5-high and ATAD5-low groups; significant differences are indicated by asterisks. (D) Heatmap of immune checkpoint gene expression across ATAD5-high and ATAD5-low groups, showing upregulation of inhibitory checkpoints including IDO1, CTLA4, CD274, LAG3, and TIGIT in ATAD5-high tumors.

ATAD5 Emerges as a CRPC-Associated Hub Gene Linked to a Plastic Malignant Cell Program

Within the MEblack module, hub genes were defined by MM > 0.7 and GS > 0.4. Among these, ATAD5 achieved the highest SCL association score of 0.89, substantially outranking other candidates including PHTF2 (0.76), DLGAP5 (0.70), and PBK (0.68) (Fig. 3A–D). Hub gene expression was consistently elevated in CRPC relative to LPCa across subtypes (Fig. 3C). Correlation analysis confirmed significant associations between ATAD5 and the stemness regulators YAP1 ($R = 0.30$, $p = 1.26 \times 10^{-46}$) and ATXN1 ($R = 0.26$, $p = 4.8 \times 10^{-35}$), further supporting ATAD5 as a stemness-associated candidate (Fig. 3E).

ATAD5 Expression Associates with Disease Progression and Poor Prognosis Across Multiple Cohorts

The prognostic relevance of ATAD5 was evaluated across multiple independent cohorts. In the SU2C/PCF cohort, high ATAD5 expression was associated with significantly shorter OS (log-rank p = 0.0012; Fig. 4A). In TCGA-PRAD, elevated ATAD5 correlated with worse PFS (p = 0.0042) and DSS (p = 0.0027), with a Cox regression forest plot confirming consistently elevated hazard ratios across OS, DFS, RFS, DSS, and PFS endpoints in all available cohorts (Fig. 4B). ATAD5 expression increased progressively

with advancing T stage ($p = 0.00022$), nodal involvement ($p = 0.0059$), higher Gleason score ($p = 6.8 \times 10^{-7}$), and abnormal PSA ($p = 0.021$) in TCGA-PRAD (Fig. 4C). These findings were further corroborated in the DKFZ2018 (relapse-free survival, $p = 0.0019$) and ICGC cohorts (OS, $p = 0.018$) (Fig. 4D).

Single-Cell Analysis Localizes ATAD5 to Malignant Epithelial Cells

To resolve ATAD5 expression at cellular resolution, scRNA-seq data from six prostate cancer patients were analyzed. Cells were annotated into seven major populations including epithelial, myeloid, T cell, B cell, CAF, endothelial, and other types (Fig. 5A–B). CNV inference using inferCNV identified malignant epithelial cells based on elevated CNV scores and positive CNV correlation relative to T/B cell references (Fig. 5C–D). ATAD5 expression was predominantly localized to the malignant epithelial compartment, with ATAD5-high cells forming a spatially distinct subpopulation on tSNE and UMAP embeddings (Fig. 5E).

ATAD5-High Malignant Epithelial Cells Display a Plasticity-Associated State and Predicted Microenvironmental Interactions

Within malignant epithelial cells, ATAD5-high cells exhibited significantly elevated SCL scores compared to ATAD5-low cells ($p < 0.0001$; Fig. 6A–B). Pseudotime trajectory analysis showed that ATAD5-high cells were enriched at later pseudotime states and maintained higher SCL scores along the inferred trajectory, suggesting progressive acquisition of stemness features during tumor evolution (Fig. 6C–D). Pathway enrichment analysis revealed that ATAD5-high cells were enriched in angiogenesis, T cell activation regulation, leukocyte adhesion, and cytokine-mediated signaling pathways (Fig. 6E). CellChat analysis demonstrated that ATAD5-high malignant epithelial cells exhibited greater predicted interaction strength and higher numbers of interactions with CAFs and myeloid cells compared to ATAD5-low cells (Fig. 6F–G), suggesting active remodeling of the tumor microenvironment by ATAD5-high cells.

Spatial and Tissue-Level Analyses Support ATAD5 Association with Epithelial and Microenvironmental Features

Spatial transcriptomic analysis of PDA and non-PDA prostate tissue sections demonstrated that ATAD5 expression was enriched in epithelial tumor regions of PDA tissues, with spatial co-enrichment of CD44, FAP, and CD8A (Fig. 7C–D). ATAD5-high epithelial microenvironments in PDA tissues were associated with significantly higher fibroblast and T cell infiltration compared to ATAD5-low regions ($p < 0.001$; Fig. 7B). IHC staining of clinical specimens from 10 LPCa and 10 CRPC patients confirmed that ATAD5,

CD44, CD8A, and FAP protein expression were all significantly elevated in CRPC relative to LPCa (all $p < 0.01$; Fig. 8A–B), corroborating the computational findings at the tissue level.

ATAD5 Knockdown Impairs Invasion and Clonogenicity in CRPC Cell Lines

Western blotting across six prostate cancer cell lines showed that ATAD5 protein was most abundantly expressed in C4-2 and 22Rv1, both castration-resistant models (Fig. 9A). Three siRNAs were tested in both cell lines, with siRNA-3 demonstrating the most efficient knockdown and selected for functional studies (Fig. 9B). Transwell assays showed that ATAD5 depletion significantly reduced cell invasion in both C4-2 and 22Rv1 cells compared to siNC controls ($p < 0.05$; Fig. 9C–D). Colony formation assays demonstrated a marked reduction in colony numbers following ATAD5 knockdown in both cell lines ($p < 0.05$; Fig. 9E–F), indicating that ATAD5 supports invasive and clonogenic capacity in CRPC cells.

Discussion

In this study, we integrated bulk transcriptomic, single-cell, spatial transcriptomic, clinical, tissue-level, and functional data to characterize ATAD5 in CRPC. ATAD5 was identified as a hub gene within a CRPC-associated co-expression program enriched for DNA replication- and stemness-related transcriptional features. Across independent cohorts, higher ATAD5 expression was associated with adverse clinical outcomes and advanced clinicopathological characteristics. Single-cell analysis localized ATAD5 predominantly to malignant epithelial cells and showed that ATAD5-high cells exhibited higher stemness-like scores and distinct pseudotime distributions. These findings suggest that ATAD5 marks a malignant epithelial state with features of increased cellular plasticity rather than establishing ATAD5 as a direct regulator of stemness. ATAD5-high tumors also displayed stromal and immune features consistent with an immunosuppressive microenvironment, while functional experiments showed that ATAD5 depletion reduced invasion and colony formation in CRPC cell models. Through WGCNA of integrated bulk transcriptomic data, the MEblack co-expression module demonstrated the strongest positive correlation with CRPC status and was enriched in stemness and DNA replication-related gene sets. Within this module, ATAD5 emerged as the top-ranked hub gene by SCL association score (0.89). High ATAD5 expression was consistently associated with adverse survival outcomes across TCGA-PRAD, SU2C/PCF, DKFZ, and ICGC cohorts, and correlated positively with advancing T stage, nodal involvement, higher Gleason score, and elevated PSA. At single-cell resolution, ATAD5 was predominantly expressed in malignant epithelial cells displaying elevated SCL scores and late pseudotime enrichment. ATAD5-high malignant cells exhibited enhanced predicted interactions with CAFs and myeloid cells. Spatial transcriptomics and immunohistochemistry corroborated these findings at the tissue level, and ATAD5 depletion impaired invasion and colony formation in C4-2 and 22Rv1 CRPC cell lines. The identification of ATAD5 as the highest-ranked hub gene within a CRPC-associated stemness module is consistent with the established understanding that CRPC progression involves the acquisition of stem-like transcriptional states beyond AR reactivation [16, 17]. Androgen deprivation selectively enriches for

stem-like cells with enhanced self-renewal and therapeutic tolerance [16], and coordinated activation of epigenetic reprogramming, Wnt/β-catenin, and Hippo pathway signaling has been implicated in sustaining these states [18, 19, 21]. The MEblack module, enriched in RAMALHO_STEMNESS_UP and GOBP_POSITIVE_REGULATION_OF_STEM_CELL_POPULATION_MAINTENANCE programs, likely reflects such a coordinated stemness transcriptional program in CRPC. ATAD5's significant correlations with stemness regulators YAP1 and ATXN1 at the transcriptomic level, together with its highest SCL association score among all module hub genes, further support its candidate association with this program. Luminal stem-like cell populations in high-risk prostate cancer have been shown to promote hormonal therapy resistance [22], and single-cell and machine learning-based approaches have linked cancer stem cell gene signatures with prostate cancer prognosis [23], collectively contextualizing the clinical relevance of stemness-associated transcriptional states in CRPC. The multi-cohort prognostic analyses demonstrated consistent associations between high ATAD5 expression and shorter PFS, DSS, OS, and relapse-free survival, as well as progressive enrichment of ATAD5 expression with advancing clinicopathological features. A growing body of literature supports transcriptomic co-expression signatures as clinically informative in prostate cancer [15, 46, 50], and our findings across four independent cohorts suggest that ATAD5 warrants further evaluation as a prognostic candidate. We note that multivariable Cox regression analysis incorporating standard clinicopathological covariates was not performed in the present study, and ATAD5 should therefore be regarded as a candidate prognostic-associated gene rather than an established independent prognostic factor. At single-cell resolution, ATAD5 expression was concentrated within the malignant epithelial compartment, and ATAD5-high cells were enriched at later pseudotime states with higher SCL scores, suggesting that ATAD5 expression may mark a more advanced stem-like state within the malignant epithelial hierarchy. This is consistent with single-cell studies identifying lineage plasticity-related cancer cell populations that contribute to prostate cancer progression [48], and with the principle that malignant cell-specific transcriptional programs are more accurately resolved at single-cell than bulk resolution [46, 47, 49]. Pathway enrichment in ATAD5-high malignant cells further implicated immune-modulatory programs including angiogenesis, T cell activation regulation, and cytokine-mediated signaling, supporting a potential role for these cells in active TME remodeling. The immunosuppressive microenvironmental features associated with high ATAD5 expression are consistent with established characteristics of the CRPC TME. Reduced cytotoxic T cell infiltration, elevated CAF enrichment, and upregulation of checkpoint molecules including IDO1, CTLA4, CD274, LAG3, and TIGIT were observed in ATAD5-high tumors. CAF-mediated signaling has been shown to regulate prostate cancer stemness and promote CRPC progression [33], and distinct CAF subpopulations contribute to immune exclusion through stromal remodeling [40, 41]. Myeloid-mediated immunosuppression represents a mechanistically characterized barrier to CRPC immunotherapy response [34], while checkpoint molecule upregulation reflects the broader immunosuppressive transcriptional landscape observed in CRPC [35, 36, 38]. CellChat analysis further predicted that ATAD5-high malignant epithelial cells exhibit stronger and more numerous interactions with CAFs and myeloid cells than ATAD5-low cells, suggesting potential involvement of ATAD5-high tumor cells in establishing this immunosuppressive niche, though causal directionality requires direct experimental validation. The elevated CD8A protein expression observed in CRPC relative to localized prostate cancer tissues by IHC

requires careful interpretation. Increased CD8A immunoreactivity reflects greater abundance of CD8A-expressing cells, but does not indicate functional cytotoxic activity. Given the concurrent upregulation of multiple inhibitory checkpoint molecules in ATAD5-high tumors and the xCell-based finding of reduced cytotoxic T cell function-related signatures, CD8A-positive cells in CRPC may represent dysfunctional or exhausted T cells within an immunosuppressive stromal context, consistent with observations in the CRPC immune landscape [36, 37, 39, 40].The molecular biology of ATAD5 provides a biologically plausible basis for its association with CRPC-related transcriptional programs. ATAD5 mediates PCNA unloading and participates in DNA damage response, including through interaction with BAZ1B and contributions to DNA repair [42, 43], and its depletion sensitizes cells to PARP inhibition [43]. Germline ATAD5 variants have been identified in breast and ovarian cancer patients [44], implicating ATAD5 dysregulation in genome instability across tumor types. The MEblack module in which ATAD5 resides was enriched in DNA replication programs, consistent with ATAD5's established molecular functions. Replication stress tolerance and enhanced DNA repair capacity are recognized features of stem-like cancer cells [20, 22], providing a potential mechanistic link between ATAD5 known biology and the stemness-associated transcriptional state observed in ATAD5-high malignant epithelial cells. We emphasize, however, that the present study did not directly assess DNA replication dynamics, PCNA loading status, replication fork activity, or downstream DNA damage signaling in CRPC cells, and the mechanistic basis of ATAD5 association with stemness programs therefore remains to be directly established. Functionally, siRNA-mediated ATAD5 depletion significantly impaired cell invasion and colony formation in both C4-2 and 22Rv1 CRPC cell lines, providing in vitro evidence consistent with a contributory role of ATAD5 in maintaining the invasive and clonogenic phenotype of CRPC cells. These functional properties are recognized hallmarks of stem-like cancer cells [20, 23], and their reduction following ATAD5 knockdown aligns with the stemness-associated transcriptional identity of ATAD5-high malignant epithelial cells observed at the single-cell level. IHC validation confirmed that ATAD5, alongside CD44, FAP, and CD8A, was significantly elevated at the protein level in CRPC relative to localized prostate cancer tissues, providing histological corroboration of the computational findings. We note that functional experiments employed transient siRNA-mediated knockdown without ATAD5 re-expression rescue experiments and without in vivo validation, limiting mechanistic conclusions. Spatial transcriptomic data were derived from PDA and non-PDA prostate tissue sections rather than a direct CRPC versus localized prostate cancer comparison, and spatial findings should therefore be interpreted as exploratory. Several additional limitations warrant acknowledgment. The discovery analyses were performed on publicly available bulk transcriptomic datasets, and single-cell and spatial datasets were derived from relatively small patient cohorts. CellChat results represent computational predictions of ligand–receptor interactions and do not constitute direct evidence of functional intercellular signaling. Multivariable prognostic modeling was not performed. Future studies incorporating larger cohorts, in vivo tumor models, rescue experiments, and direct mechanistic interrogation of ATAD5 in DNA replication, stemness regulation, and TME crosstalk will be necessary to fully define its functional contributions to CRPC pathobiology and its potential translational value.

Conclusion

Through integrated bulk transcriptomic, single-cell, spatial, clinical, tissue-level, and functional analyses, we identified ATAD5 as a candidate marker of an aggressive malignant epithelial state in CRPC. Higher ATAD5 expression was associated with tumor plasticity-related transcriptional features, adverse clinical outcomes, advanced clinicopathological characteristics, and immunosuppressive microenvironmental signatures. At single-cell resolution, ATAD5 was predominantly expressed in malignant epithelial cells, and ATAD5-high cells displayed higher stemness-like scores and distinct pseudotime distributions. Tissue-level analyses supported increased ATAD5 expression in CRPC, while functional studies showed that ATAD5 depletion impaired invasion and colony formation in CRPC cell lines. These findings establish ATAD5 as a candidate biomarker associated with aggressive CRPC biology, while its causal role in tumor progression and its potential therapeutic value remain to be determined.

Abbreviations

Abbreviation
Full Term
ATAD5
ATPase family AAA domain-containing protein 5
CRPC
castration-resistant prostate cancer
SCL
stemness-like
GEO
Gene Expression Omnibus
WGCNA
weighted gene co-expression network analysis
TCGA-PRAD
The Cancer Genome Atlas Prostate Adenocarcinoma
SU2C/PCF
Stand Up ToCancer/Prostate Cancer Foundation
DKFZ
Deutsches Krebsforschungszentrum (German Cancer Research Center)
ICGC
International Cancer Genome Consortium
IHC
immunohistochemistry
siRNA
small interfering RNA
LPCa
localized prostate cancer
VST

variance-stabilizing transformation
PCA
principal component analysis
DEGs
differentially expressed genes
GSEA
Gene Set Enrichment Analysis
NES
normalized enrichment score
FDR
false discovery rate
KEGG
Kyoto Encyclopedia of Genes and Genomes
MSigDB
Molecular Signatures Database
MAD
median absolute deviation
ME
module eigengene
GS
gene significance
PFS
progression-free survival
OS
overall survival
DFS
disease-free survival
RFS
relapse-free survival
DSS
disease-specific survival
scRNA-seq
single-cell RNA sequencing
UMI
unique molecular identifier
CNV
copy number variation
tSNE
t-distributed stochastic neighbor embedding
UMAP

uniform manifold approximation and projection
PDA
prostatic ductal adenocarcinoma
FAP
fibroblast activation protein
RIPA
radioimmunoprecipitation assay
SDS-PAGE
sodium dodecyl sulfate–polyacrylamide gel electrophoresis
PVDF
polyvinylidene fluoride
TBST
Tris-buffered saline with Tween-20
HRP
horseradish peroxidase
ECL
enhanced chemiluminescence
FFPE
formalin-fixed, paraffin-embedded
PBS
phosphate-buffered saline
CSS
charcoal-stripped serum
FBS
fetal bovine serum
siNC
negative control siRNA
AR
androgen receptor
NE
neuroendocrine
GO
Gene Ontology
PSA
prostate-specific antigen

Declarations

Ethics Approval and Consent to Participate

This study was approved by the Medical Ethics Committee of The Second Hospital of Tianjin Medical University, Tianjin Institute of Urology, Tianjin, China. All procedures were performed in accordance with the Declaration of Helsinki. Informed consent was obtained from all participants prior to enrollment.

Competing interests

The authors declare that they have no competing interests.

Funding

This work was supported by National Natural Science Foundation of China (grant 82303885), sponsored by Tianjin Health Research Project (GrantNo. TJWJ2024QN018) and Tianjin Municipal Science and Technology Bureau (Grant No. 25ZXDFQY00190).

Author Contribution

Ruitao Li, Yi Zheng, and Junlin Shen contributed equally to this work. Ruitao Li performed the bioinformatic analyses and drafted the manuscript. Yi Zheng, and Junlin Shen conducted the experimental validation, including western blotting, immunohistochemistry, Transwell invasion assays, and colony formation assays. Hongli Zhang, Cheng Fang, Xiepeng Zuo, Zhen Zhou, and Pu Wang assisted with data collection and interpretation. Jianpeng Yu and Yuanjie Niu conceived and supervised the study, and critically revised the manuscript. All authors read and approved the final manuscript.

Acknowledgements

The authors thank the publicly available databases and their contributors for providing the datasets used in this study. The authors also thank all participants and colleagues who contributed to the clinical and experimental work.

Availability of Data and Materials

The datasets analyzed in this study are publicly available from the Gene Expression Omnibus (GEO), The Cancer Genome Atlas (TCGA), cBioPortal, and other relevant public databases under the accession numbers specified in the manuscript. Additional datasets and materials generated or analyzed during the current study are available from the corresponding author upon reasonable request and with the approval of the corresponding author.

References

1. Carlsson SV, Vickers AJ. Screening for Prostate Cancer. Med Clin N Am. 2020;104(6):1051–62. https://doi.org/10.1016/j.mcna.2020.08.007.
2. Lancia A, Zilli T, Achard V, Dirix P, Everaerts W, Gomez-Iturriaga A, Ingrosso G, Liefhooghe N, Miralbell R, Siva S, Van der Eecken K, Ost P. Oligometastatic prostate cancer: The game is afoot. Cancer Treat Rev. 2019;73:84–90. https://doi.org/10.1016/j.ctrv.2019.01.005.
3. Tidd-Johnson A, Sebastian SA, Co EL, Afaq M, Kochhar H, Sheikh M, Mago A, Poudel S, Fernandez JA, Rodriguez ID, Razdan S. Prostate cancer screening: Continued controversies and novel biomarker advancements. Curr Urol. 2022;16(4):197–206. https://doi.org/10.1097/CU9.0000000000000145.
4. Bakht MK, Yamada Y, Ku SY, Venkadakrishnan VB, Korsen JA, Kalidindi TM, Mizuno K, Ahn SH, Seo JH, Garcia MM, Khani F, Elemento O, Long HW, Chaglassian A, Pillarsetty N, Lewis JS, Freedman M, Belanger AP, Nguyen QD, Beltran H. Landscape of prostate-specific membrane antigen heterogeneity and regulation in AR-positive and AR-negative metastatic prostate cancer. Nat cancer. 2023;4(5):699–715. https://doi.org/10.1038/s43018-023-00539-6.
5. Mukherji D, Omlin A, Pezaro C, Shamseddine A, de Bono J. Metastatic castration-resistant prostate cancer (CRPC): preclinical and clinical evidence for the sequential use of novel therapeutics. Cancer Metastasis Rev. 2014;33(2–3):555–66. https://doi.org/10.1007/s10555-013-9473-1.
6. Saad F, Shore N, Zhang T, Sharma S, Cho HK, Jacobs IA. Emerging therapeutic targets for patients with advanced prostate cancer. Cancer Treat Rev. 2019;76:1–9. https://doi.org/10.1016/j.ctrv.2019.03.002.
7. Seruga B, Ocana A, Tannock IF. Drug resistance in metastatic castration-resistant prostate cancer. Nat Rev Clin Oncol. 2011;8(1):12–23. https://doi.org/10.1038/nrclinonc.2010.136.
8. Iacovelli R, Ciccarese C, Schinzari G, Rossi E, Maiorano BA, Astore S, D'Angelo T, Cannella A, Pirozzoli C, Teberino MA, Pierconti F, Martini M, Tortora G. Biomarkers of response to advanced prostate cancer therapy. Expert Rev Mol Diagn. 2020;20(2):195–205. https://doi.org/10.1080/14737159.2020.1707669.
9. Li Y, Shi H, Zhao Z, Xu M. Identification of castration-dependent and -independent driver genes and pathways in castration-resistant prostate cancer (CRPC). BMC Urol. 2022;22(1):162. https://doi.org/10.1186/s12894-022-01113-5.
10. Kotamarti S, Armstrong AJ, Polascik TJ, Moul JW. Molecular Mechanisms of Castrate-Resistant Prostate Cancer. Urologic Clin North Am. 2022;49(4):615–26. https://doi.org/10.1016/j.ucl.2022.07.005.
11. Vlachostergios PJ, Puca L, Beltran H. Emerging Variants of Castration-Resistant Prostate Cancer. Curr Oncol Rep. 2017;19(5):32. https://doi.org/10.1007/s11912-017-0593-6.
12. Vellky JE, Ricke WA. (2020). Development and prevalence of castration-resistant prostate cancer subtypes. *Neoplasia (New York, N.Y.)*, *22*(11), 566–575. https://doi.org/10.1016/j.neo.2020.09.002
13. Jamroze A, Chatta G, Tang DG. Androgen receptor (AR) heterogeneity in prostate cancer and therapy resistance. Cancer Lett. 2021;518:1–9. https://doi.org/10.1016/j.canlet.2021.06.006.

14. Zhang H, Zhou Y, Xing Z, Sah RK, Hu J, Hu H. Androgen Metabolism and Response in Prostate Cancer Anti-Androgen Therapy Resistance. Int J Mol Sci. 2022;23(21):13521. https://doi.org/10.3390/ijms232113521.
15. Han H, Lee HH, Choi K, Moon YJ, Heo JE, Ham WS, Jang WS, Rha KH, Cho NH, Giancotti FG, Choi YD. Prostate epithelial genes define therapy-relevant prostate cancer molecular subtype. Prostate Cancer Prostatic Dis. 2021;24(4):1080–92. https://doi.org/10.1038/s41391-021-00364-x.
16. Kim WK, Buckley AJ, Lee DH, Hiroto A, Nenninger CH, Olson AW, Wang J, Li Z, Vikram R, Adzavon YM, Yau TY, Bao Y, Kahn M, Geradts J, Xiao GQ, Sun Z. Androgen deprivation induces double-null prostate cancer via aberrant nuclear export and ribosomal biogenesis through HGF and Wnt activation. Nat Commun. 2024;15(1):1231. https://doi.org/10.1038/s41467-024-45489-4.
17. Ge R, Wang Z, Montironi R, Jiang Z, Cheng M, Santoni M, Huang K, Massari F, Lu X, Cimadamore A, Lopez-Beltran A, Cheng L. Epigenetic modulations and lineage plasticity in advanced prostate cancer. Annals oncology: official J Eur Soc Med Oncol. 2020;31(4):470–9. https://doi.org/10.1016/j.annonc.2020.02.002.
18. Zhang X, Li H, Wang Y, Zhao H, Wang Z, Chan FL. Nuclear receptor NURR1 functions to promote stemness and epithelial-mesenchymal transition in prostate cancer via its targeting of Wnt/β-catenin signaling pathway. Cell Death Dis. 2024;15(3):234. https://doi.org/10.1038/s41419-024-06621-w.
19. Salem O, Hansen CG. The Hippo Pathway in Prostate Cancer. Cells. 2019;8(4):370. https://doi.org/10.3390/cells8040370.
20. Zhang Y, Jin Z, Zhou H, Ou X, Xu Y, Li H, Liu C, Li B. Suppression of prostate cancer progression by cancer cell stemness inhibitor napabucasin. Cancer Med. 2016;5(6):1251–8. https://doi.org/10.1002/cam4.675.
21. Jiang C, Song Y, Rorive S, Allard J, Tika E, Zahedi Z, Dubois C, Salmon I, Sifrim A, Blanpain C. Innate immunity and the NF-κB pathway control prostate stem cell plasticity, reprogramming and tumor initiation. Nat cancer. 2025;6(9):1537–58. https://doi.org/10.1038/s43018-025-00994-3.
22. Tang G, Liu J, Gao X, Yuan K, Chen M, Wang L, Qi L, Cai Y. Luminal Stem-like Cells in High-Risk/Locally Advanced Prostate Cancer Promote Resistance to Hormonal Therapy. Theranostics. 2025;15(18):9558–79. https://doi.org/10.7150/thno.112496.
23. Wang Y, Ma L, He J, Gu H, Zhu H. Identification of cancer stem cell-related genes through single cells and machine learning for predicting prostate cancer prognosis and immunotherapy. Front Immunol. 2024;15:1464698. https://doi.org/10.3389/fimmu.2024.1464698.
24. Yasumizu, Y., Rajabi, H., Jin, C., Hata, T., Pitroda, S., Long, M. D., Hagiwara, M.,Li, W., Hu, Q., Liu, S., Yamashita, N., Fushimi, A., Kui, L., Samur, M., Yamamoto,M., Zhang, Y., Zhang, N., Hong, D., Maeda, T., Kosaka, T., … Kufe, D. (2020). MUC1-C regulates lineage plasticity driving progression to neuroendocrine prostate cancer.Nature communications, 11(1), 338. https://doi.org/10.1038/s41467-019-14219-6.

25. Massari F, Maines F, Modena A, Brunelli M, Bria E, Artibani W, Martignoni G, Tortora G. Castration resistant prostate cancer (CRPC): state of the art, perspectives and new challenges. Anti-cancer Agents Med Chem. 2013;13(6):872–86. https://doi.org/10.2174/18715206113139990077.
26. Kaarijärvi R, Kaljunen H, Nappi L, Fazli L, Kung SHY, Hartikainen JM, Paakinaho V, Capra J, Rilla K, Malinen M, Mäkinen PI, Ylä-Herttuala S, Zoubeidi A, Wang Y, Gleave ME, Hiltunen M, Ketola K. DPYSL5 is highly expressed in treatment-induced neuroendocrine prostate cancer and promotes lineage plasticity via EZH2/PRC2. Commun biology. 2024;7(1):108. https://doi.org/10.1038/s42003-023-05741-x.
27. Taher A, Jensen CT, Yedururi S, Surasi DS, Faria SC, Bathala TK, Mujtaba B, Bhosale P, Wagner-Bartak N, Morani AC. Imaging of Neuroendocrine Prostatic Carcinoma. Cancers. 2021;13(22):5765. https://doi.org/10.3390/cancers13225765.
28. Pitzen, S. P., Rudenick, A. N., Qiu, Y., Zhang, W., Munro, S. A., McCluskey, B. M.,Forster, C., Bergom, H. E., Ali, A., Boytim, E., Lafin, J. T., Linder, S., Ismail,M., Devlies, W., Sessions, C. J., Claessens, F., Joniau, S., Attard, G., Zwart, W.,Nelson, P. S., … Dehm, S. M. (2025). Comparative transcriptomics reveals a mixed basal,club, and hillock epithelial cell identity in castration-resistant prostate cancer.Proceedings of the National Academy of Sciences of the United States of America, 122(6), e2415308122. https://doi.org/10.1073/pnas.2415308122.
29. Brevi, A., Lorenzoni, M., Caputo, S., Yamada, Y., Grioni, M., Cogrossi, L. L., Martinez-Vidal,L., Cassina, V., Cipria, D., Venegoni, C., Zordan, P., Matafora, V., Tascini, A. S.,Tenace, N. P., Campanile, R., Cucchiara, V., Pinna, V., Jachetti, E., Galli, R., Bachi,A., … Bellone, M. (2026). Intercepting YAP Activation in Prostate Cancer Blocks Neuroendocrine Progression. Cancer research, 86(12), 2860–2877. https://doi.org/10.1158/0008-5472.CAN-25-2704.
30. Dwivedi S, Bautista M, Shrestha S, Elhasasna H, Chaphekar T, Vizeacoumar FS, Krishnan A. Sympathetic signaling facilitates progression of neuroendocrine prostate cancer. Cell death discovery. 2021;7(1):364. https://doi.org/10.1038/s41420-021-00752-1.
31. Guo, C., Crespo, M., Gurel, B., Dolling, D., Rekowski, J., Sharp, A., Petremolo, A.,Sumanasuriya, S., Rodrigues, D. N., Ferreira, A., Pereira, R., Figueiredo, I., Mehra,N., Lambros, M. B. K., Neeb, A., Gil, V., Seed, G., Terstappen, L., Alimonti, A.,Drake, C. G., … International SU2C PCF Prostate Cancer Dream Team (2021). CD38 in Advanced Prostate Cancers. European urology, 79(6), 736–746. https://doi.org/10.1016/j.eururo.2021.01.017.
32. Cha HR, Lee JH, Ponnazhagan S. Revisiting Immunotherapy: A Focus on Prostate Cancer. Cancer Res. 2020;80(8):1615–23. https://doi.org/10.1158/0008-5472.CAN-19-2948.
33. Chen H, Li Z, Yue Y, Zhu X, Wang J, Chen Y, Wang Y, Luo Z, Liu H. CAF-mediated regulation of prostate cancer stem cell stemness via the Wnt/β-catenin and SDF-1/CXCR4 pathways in castration-resistant prostate cancer. Front cell Dev biology. 2025;13:1617200. https://doi.org/10.3389/fcell.2025.1617200.
34. Lyu A, Fan Z, Clark M, Lea A, Luong D, Setayesh A, Starzinski A, Wolters R, Arias-Badia M, Allaire K, Wu K, Gurunathan V, Valderrábano L, Wei XX, Miller RA, Van Allen EM, Fong L. Evolution of myeloid-

mediated immunotherapy resistance in prostate cancer. Nature. 2025;637(8048):1207–17. https://doi.org/10.1038/s41586-024-08290-3.

35. Xue D, Zuo Q, Chang J, Wu X. The correlation between TRIM28 expression and immune checkpoints in CRPC. FASEB journal: official publication Federation Am Soc Experimental Biology. 2024;38(13):e23663. https://doi.org/10.1096/fj.202400061RR.
36. Hansen SB, Unal B, Kuzu OF, Saatcioglu F. Immunological facets of prostate cancer and the potential of immune checkpoint inhibition in disease management. Theranostics. 2024;14(18):6913–34. https://doi.org/10.7150/thno.100555.
37. Conteduca, V., Caffo, O., Scarpi, E., Sepe, P., Galli, L., Fratino, L., Maines, F.,Chiuri, V. E., Santoni, M., Zanardi, E., Massari, F., Toma, I., Lolli, C., Schepisi,G., Sbrana, A., Kinspergher, S., Cursano, M. C., Casadei, C., Modonesi, C., Santini,D., … De Giorgi, U. (2020). Immune Modulation in Prostate Cancer Patients Treated with Androgen Receptor (AR)-Targeted Therapy. Journal of clinical medicine, 9(6), 1950. https://doi.org/10.3390/jcm9061950.
38. Sridaran D, Bradshaw E, DeSelm C, Pachynski R, Mahajan K, Mahajan NP. Prostate cancer immunotherapy: Improving clinical outcomes with a multi-pronged approach. Cell Rep Med. 2023;4(10):101199. https://doi.org/10.1016/j.xcrm.2023.101199.
39. Gu Y, Wei F, Dong Y, Lin X, Su Y, Wood G, Seidah NG, Bonert M, Werstuck G, Aziz T, Major, P., Tang D. (2026). PCSK9 promotes prostate cancer via facilitating intratumoral cholesterol accumulation and enhancing immunosuppressive tumor microenvironment. *Journal of advanced research*, S2090-1232(26)00299-7. Advance online publication. https://doi.org/10.1016/j.jare.2026.04.020
40. Qiu Y, Wang Y, Liu J, Sun K, Liu B, Hou Q. Single-cell sequencing unveils the transcriptomic landscape of castration-resistant prostate cancer-associated fibroblasts and their association with prognosis and immunotherapy response. BMC Cancer. 2025;25(1):813. https://doi.org/10.1186/s12885-025-14212-x.
41. He K, Zhao Z, Bai J, Lu T, Hu Y, He X, Wei F, Zhang Y, Gu Y, Shi Z, Meng X, Wang F, Shi C, Qin W, Zhang K, Xie Q, Yang L. The Role of Distinct Cancer-Associated Fibroblast Subtypes in Prostate Cancer Immunotherapy. Int J Biol Sci. 2026;22(13):7259–76. https://doi.org/10.7150/ijbs.132227.
42. Kim Y, Ha NY, Kang MS, Ryu E, Yi G, Yoo J, Kang N, Kim BG, Myung K, Kang S. ATAD5-BAZ1B interaction modulates PCNA ubiquitination during DNA repair. Nat Commun. 2024;15(1):10496. https://doi.org/10.1038/s41467-024-55005-3.
43. Giovannini S, Weller MC, Hanzlíková H, Shiota T, Takeda S, Jiricny J. ATAD5 deficiency alters DNA damage metabolism and sensitizes cells to PARP inhibition. Nucleic Acids Res. 2020;48(9):4928–39. https://doi.org/10.1093/nar/gkaa255.
44. Maleva Kostovska I, Wang J, Bogdanova N, Schürmann P, Bhuju S, Geffers R, Dürst M, Liebrich C, Klapdor R, Christiansen H, Park-Simon TW, Hillemanns P, Plaseska-Karanfilska D, Dörk T. Rare ATAD5 missense variants in breast and ovarian cancer patients. Cancer Lett. 2016;376(1):173–7. https://doi.org/10.1016/j.canlet.2016.03.048.

45. Fox JT, Sakamuru S, Huang R, Teneva N, Simmons SO, Xia M, Tice RR, Austin CP, Myung K. High-throughput genotoxicity assay identifies antioxidants as inducers of DNA damage response and cell death. Proc Natl Acad Sci USA. 2012;109(14):5423–8. https://doi.org/10.1073/pnas.1114278109.
46. Song H, Weinstein HNW, Allegakoen P, Wadsworth MH 2nd, Xie J, Yang H, Castro EA, Lu KL, Stohr BA, Feng FY, Carroll PR, Wang B, Cooperberg MR, Shalek AK, Huang FW. Single-cell analysis of human primary prostate cancer reveals the heterogeneity of tumor-associated epithelial cell states. Nat Commun. 2022;13(1):141. https://doi.org/10.1038/s41467-021-27322-4.
47. Kfoury Y, Baryawno N, Severe N, Mei S, Gustafsson K, Hirz T, Brouse T, Scadden EW, Igolkina AA, Kokkaliaris K, Choi BD, Barkas N, Randolph MA, Shin JH, Saylor PJ, Scadden DT, Sykes DB, Kharchenko PV, Boston Bone Metastases Consortium. Human prostate cancer bone metastases have an actionable immunosuppressive microenvironment. Cancer Cell. 2021;39(11):1464–e14788. https://doi.org/10.1016/j.ccell.2021.09.005. & as part of the.
48. Zhao F, Zhang T, Wei J, Chen L, Liu Z, Jin Y, Liu M, Zhou H, Hu Y, Sheng X. Integrated single-cell transcriptomic analyses identify a novel lineage plasticity-related cancer cell type involved in prostate cancer progression. EBioMedicine. 2024;109:105398. https://doi.org/10.1016/j.ebiom.2024.105398.
49. Yu X, Liu R, Gao W, Wang X, Zhang Y. Single-cell omics traces the heterogeneity of prostate cancer cells and the tumor microenvironment. Cell Mol Biol Lett. 2023;28(1):38. https://doi.org/10.1186/s11658-023-00450-z.
50. Mou Z, Harries LW. Integration of single-cell and bulk RNA-sequencing data reveals the prognostic potential of epithelial gene markers for prostate cancer. Mol Oncol. 2025;19(6):1811–35. https://doi.org/10.1002/1878-0261.13804.
51. Howells M, Gangadharannambiar P, McMullen C, Crea F, Bacon W, Christiansen C. Characterizing resistance in prostate cancer at a single cell level with hormonal treatment and epigenetic inhibitors. J Pharm Pharmacol. 2026;78(2):rgaf100. https://doi.org/10.1093/jpp/rgaf100.
52. Fang R, Zhao S, Si M, Zhang Y, Xu R, Li J. Heterogeneity and prognostic significance of mast cell subsets in the tumor microenvironment of prostate cancer. Cancer Immunol immunotherapy: CII. 2026;75(4):118. https://doi.org/10.1007/s00262-026-04363-6.
53. Kiviaho, A., Eerola, S. K., Kallio, H. M. L., Andersen, M. K., Hoikka, M., Tiihonen,A. M., Salonen, I., Spotbeen, X., Giesen, A., Parker, C. T. A., Taavitsainen, S.,Hantula, O., Marttinen, M., Hermelo, I., Ismail, M., Midtbust, E., Wess, M., Devlies,W., Sharma, A., Krossa, S., … Nykter, M. (2024). Single cell and spatial transcriptomics highlight the interaction of club-like cells with immunosuppressive myeloid cells in prostate cancer. Nature communications, 15(1), 9949. https://doi.org/10.1038/s41467-024-54364-1.
54. Bian X, Wang W, Abudurexiti M, Zhang X, Ma W, Shi G, Du L, Xu M, Wang X, Tan C, Sun H, He X, Zhang C, Zhu Y, Zhang M, Ye D, Wang J. (2024). Integration Analysis of Single-Cell Multi-Omics Reveals Prostate Cancer Heterogeneity. *Advanced science (Weinheim, Baden-Wurttemberg, Germany)*, *11*(18), e2305724. https://doi.org/10.1002/advs.202305724

55. Yu H, Wang Y, He M, Chen Y, Bi J, Lin X, Cui X. Integrated single-cell and spatial transcriptomic profiling decodes lineage plasticity and immune microenvironment remodeling in prostate cancer progression. Mol Cancer. 2026;25(1):88. https://doi.org/10.1186/s12943-026-02617-6.
56. Feng DC, Zhu WZ, Wang J, Li DX, Shi X, Xiong Q, You J, Han P, Qiu S, Wei Q, Yang L. The implications of single-cell RNA-seq analysis in prostate cancer: unraveling tumor heterogeneity, therapeutic implications and pathways towards personalized therapy. Military Med Res. 2024;11(1):21. https://doi.org/10.1186/s40779-024-00526-7.
57. Ali A, Mikutenaite M, Weischenfeldt J, Bristow RG. Single-cell and spatial RNA sequencing in prostate cancer. Nat Rev Urol. 2026. 10.1038/s41585-026-01149-4. Advance online publication.

Figures

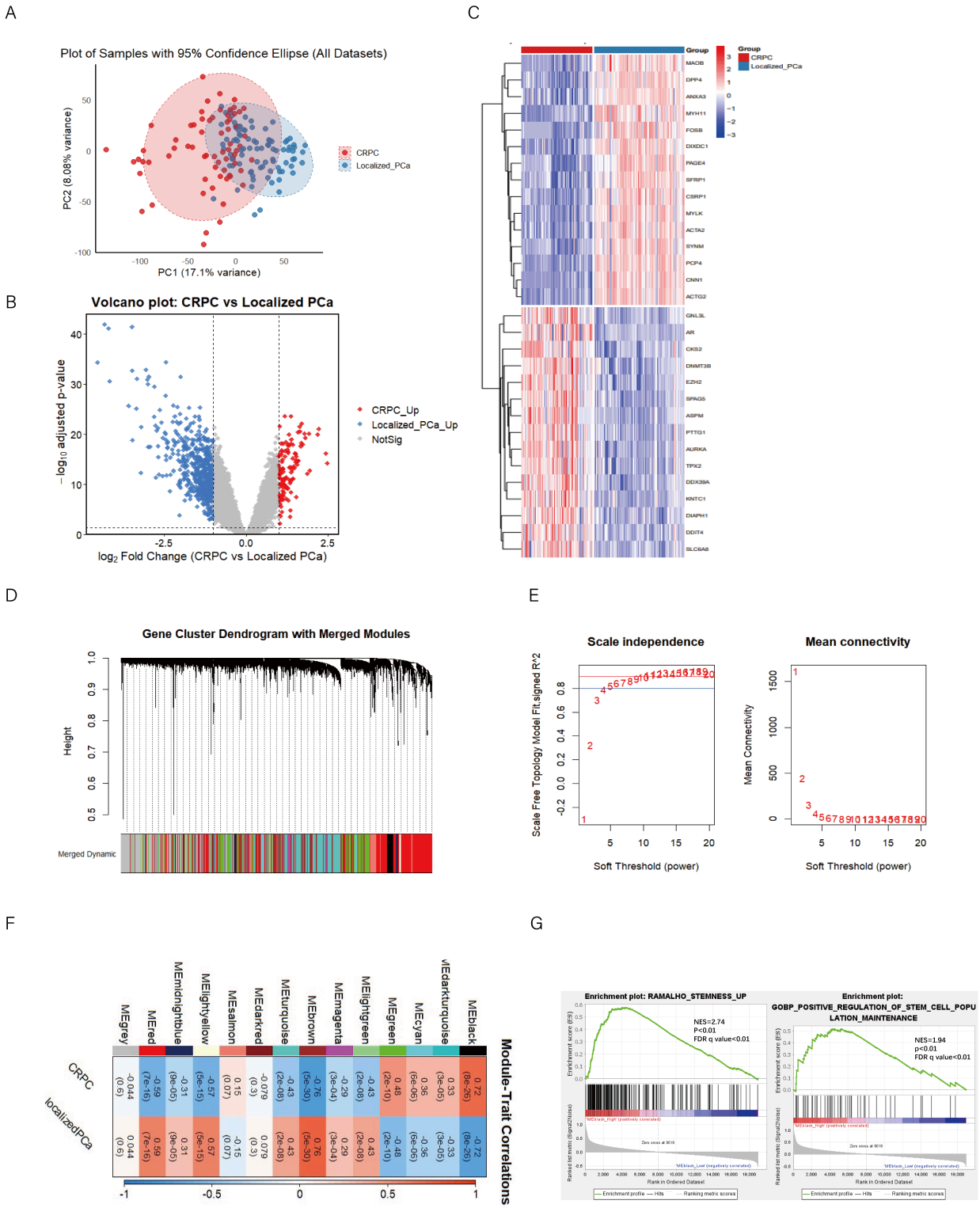


Figure 1

Identification of a CRPC-associated stemness transcriptional program by integrated transcriptomic analysis and WGCNA. (A) PCA plot showing separation of CRPC (red) and localized prostate cancer (LPCa, blue) samples across integrated datasets, with PC1 explaining 17.1% and PC2 explaining 8.08% of total variance. (B) Volcano plot of differentially expressed genes between CRPC and LPCa ($|\log_2 FC| > 1$, $p < 0.05$); red and blue dots indicate genes upregulated in CRPC and LPCa, respectively. (C)Heatmap

of top differentially expressed genes, hierarchically clustered by expression pattern across CRPC and LPCa samples. (D) Gene cluster dendrogram with merged co-expression modules identified by WGCNA. (E) Soft-thresholding power selection plots showing scale-free topology fit index and mean connectivity; power = 4 was selected. (F) Module-trait correlation heatmap; MEblack showed the strongest positive correlation with CRPC status (r=0.72). (G) GSEA enrichment plots for RAMALHO_STEMNESS_UP(NES=2.74,FDRq<0.01)and GOBP_POSITIVE_REGULATION_OF_STEM_CELL_POPULATION_MAINTENANCE (NES = 1.94, FDR q < 0.01) within the MEblack module.

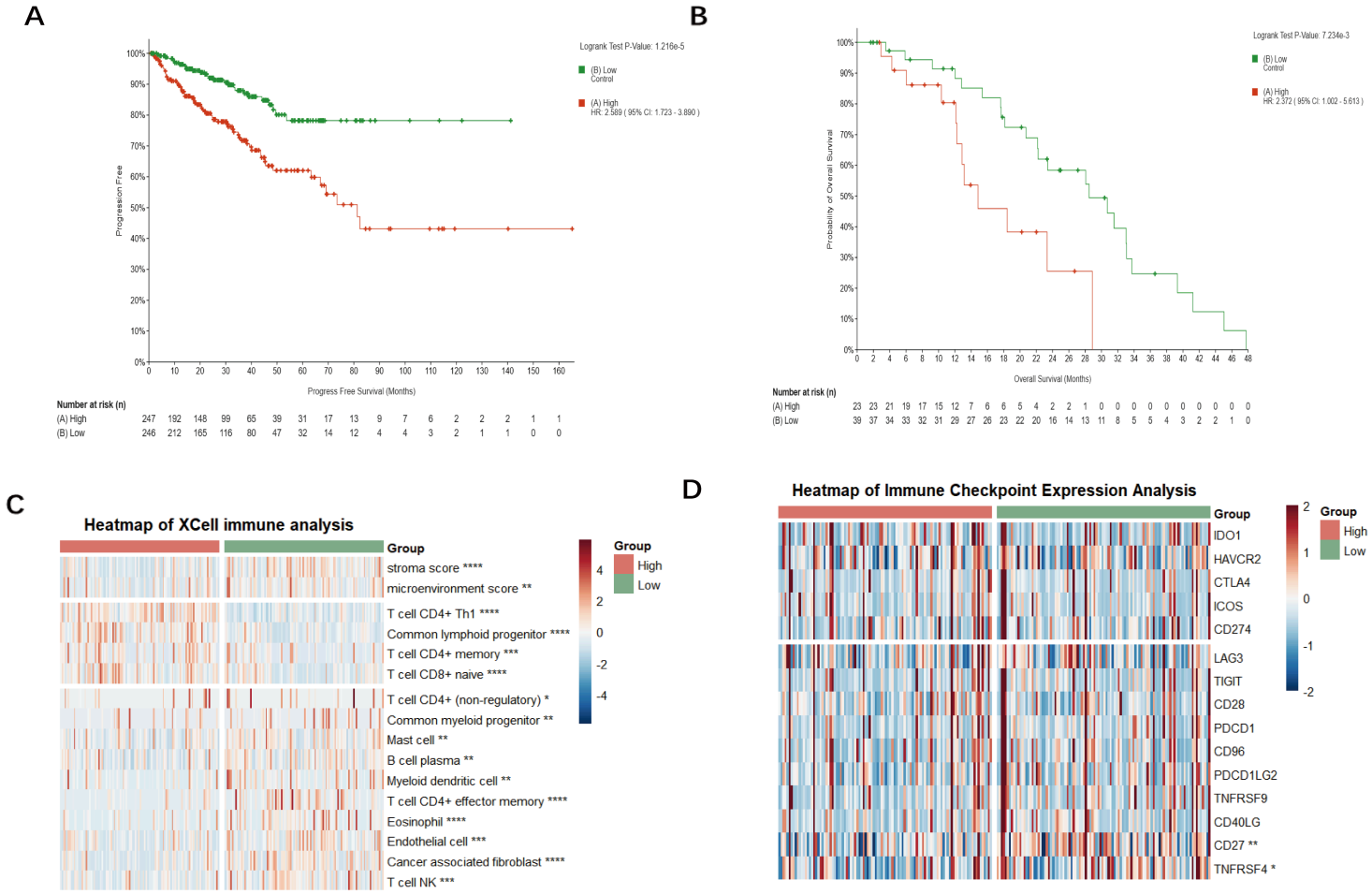


Figure 2

High MEblack module expression is associated with adverse survival outcomes and an immunosuppressive tumor microenvironment.

(A) Kaplan–Meier curve for progression-free survival (PFS) stratified by MEblack eigengene score in the TCGA-PRAD cohort (log-rank p =1.22 ×10^{-5}; HR =2.569, 95% CI: 1.723–3.890). (B) Kaplan–Meier curve for overall survival (OS) stratified by MEblack eigengene score in the SU2C/PCF cohort (log-rank p=7.23 ×10^{-3}; HR = 2.372, 95% CI: 1.002–5.613). (C)Heatmap of xCell immune infiltration scores across ATAD5-high and ATAD5-low groups; significant differences are indicated by asterisks. (D) Heatmap of immune

checkpoint gene expression across ATAD5-high and ATAD5-low groups, showing upregulation of inhibitory checkpoints including IDO1, CTLA4, CD274, LAG3, and TIGIT in ATAD5-high tumors.

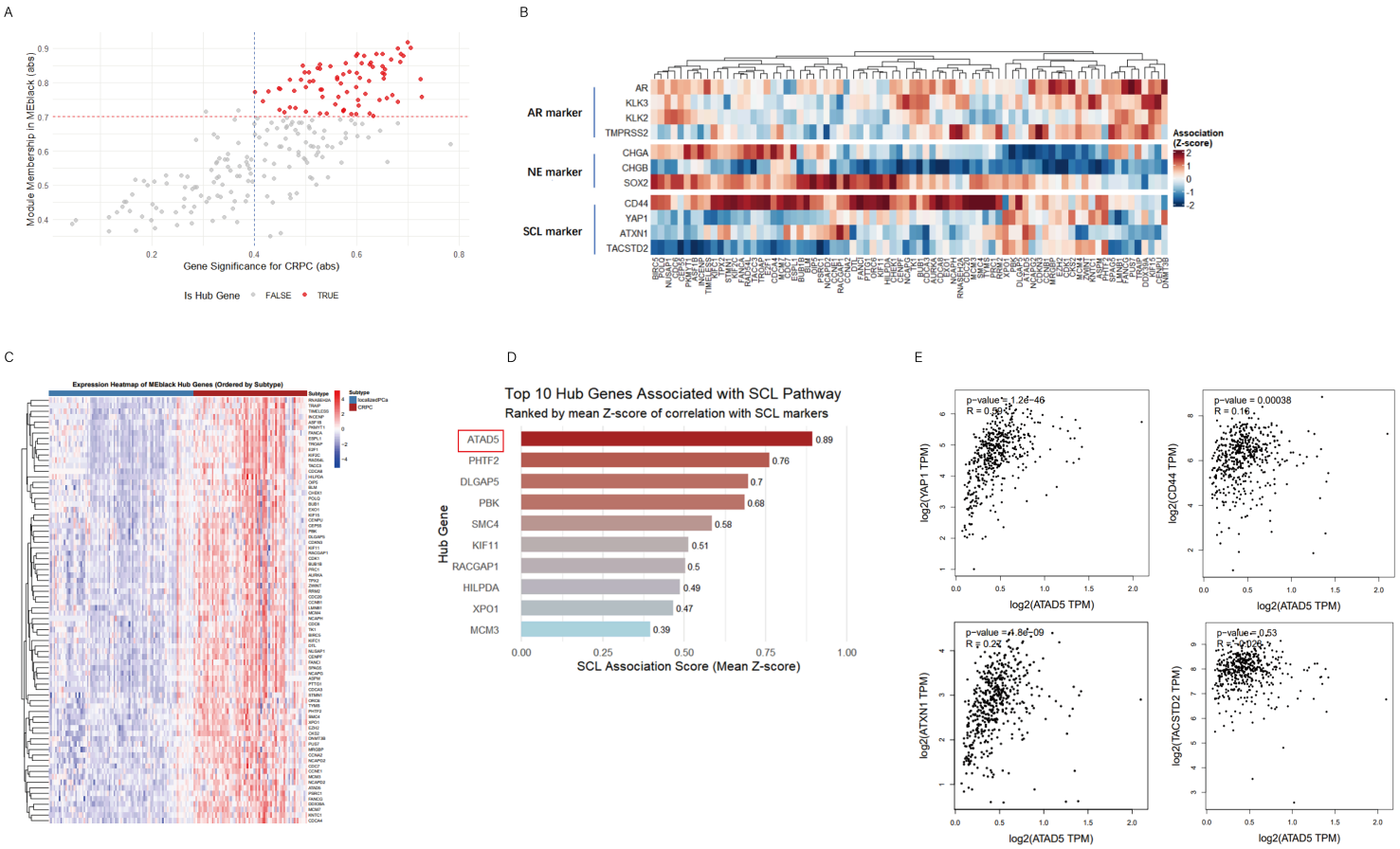


Figure 3

ATAD5 is identified as the top stemness-associated hub gene in the MEblack module. (A) Scatter plot of module membership (MM) versus gene significance (GS) for MEblack module genes; hub genes (MM > 0.7, GS > 0.4) are highlighted in red. (B) Heatmap showing correlation of hub genes with AR, neuroendocrine (NE), and stemness-like (SCL) markers across MEblack hub genes. (C) Expression heatmap of MEblack hub genes ordered by prostate cancer subtype (LPCa vs. CRPC). (D) Bar chart of the top 10 hub genes ranked by SCL association score; ATAD5 ranks first with a score of 0.89. (E) Scatter plots showing correlations between ATAD5 expression and SCL markers YAP1 (R = 0.30, p = 1.26×10^{-46}), CD44 (p = 0.00038), ATXN1 (R = 0.26, p = 4.8×10^{-35}), and TACSTD2 (p = 0.53).

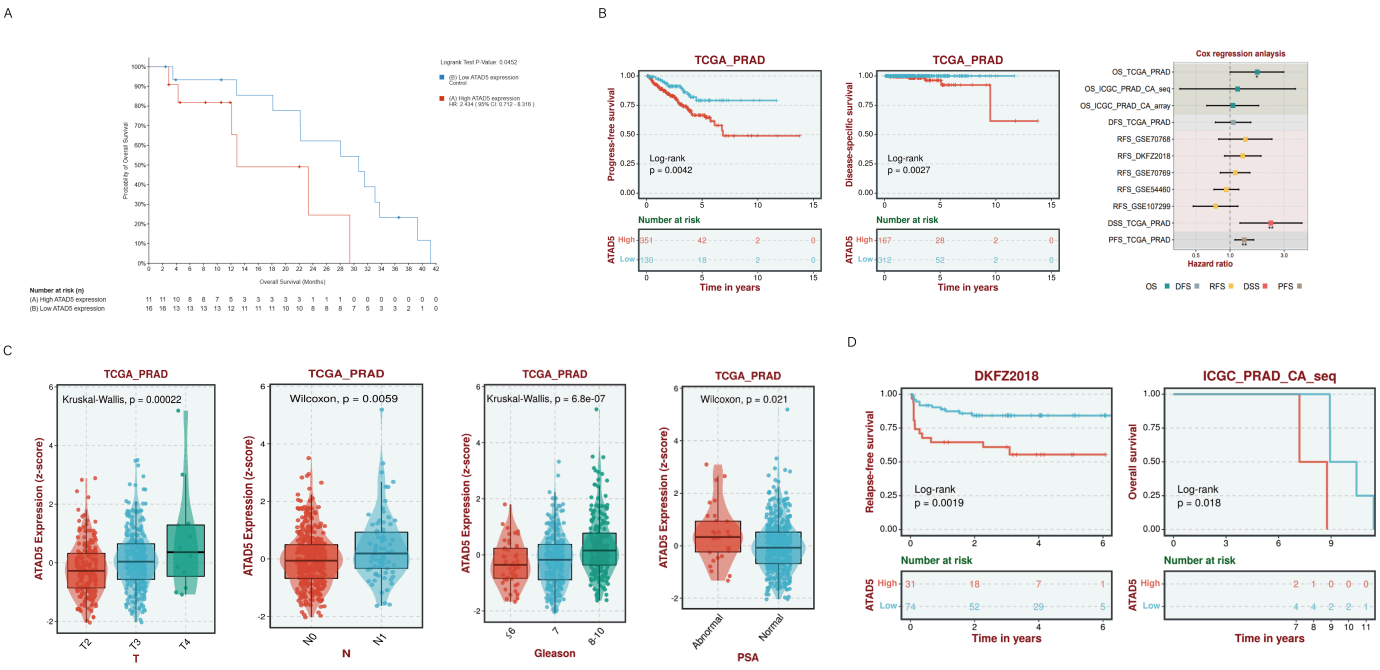


Figure 4

ATAD5 expression correlates with prostate cancer progression and predicts adverse clinical outcomes across independent cohorts. (A) Kaplan–Meier curve for OS stratified by ATAD5 expression in the SU2C/PCF cohort (log-rank p = 0.0012). (B) Kaplan–Meier curves for PFS (log-rank p = 0.0042) and disease-specific survival (DSS; log-rank p = 0.0027) in TCGA-PRAD, and Cox regression forest plot summarizing hazard ratios across multiple independent cohorts for OS, DFS, RFS, DSS, and PFS endpoints. (C) Box plots showing ATAD5 expression across T stage (p = 0.00022), N stage (p = 0.0059), Gleason score (p = 6.8 × 10^{-7}), and PSA status (p = 0.021) in TCGA-PRAD. (D) Kaplan–Meier curves for relapse-free survival in DKFZ2018 (log-rank p = 0.0019) and OS in ICGC_PRAD_CA_seq (log-rank p = 0.018).

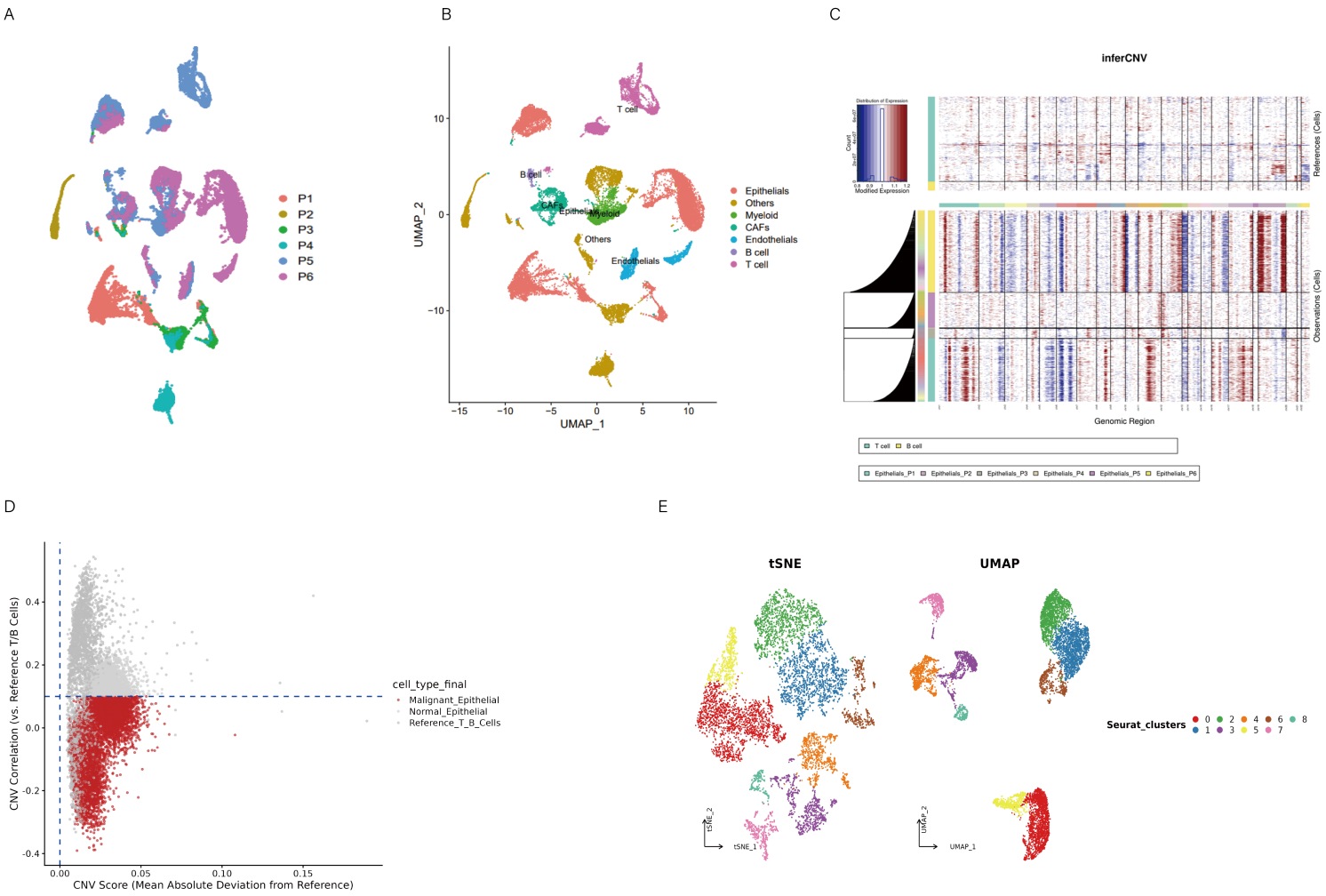


Figure 5

Single-cell RNA sequencing identifies ATAD5 as predominantly expressed in malignant epithelial cells. (A) UMAP plot of six CRPC patients (P1–P6) showing patient-level distribution of cells. (B) UMAP plot with cell type annotation, including epithelial, myeloid, T cell, B cell,CAFs, endothelial, and other populations. (C)inferCNV heatmap displaying copy number variation profiles across epithelial cells from six patients and reference T/B cells across genomic regions. (D) Scatter plot of CNV score versus CNV correlation used to classify malignant epithelial cells (red) and normal epithelial cells (grey), with reference T/B cells shown separately. (E) tSNE and UMAP plots of malignant epithelial cells colored by Seurat cluster, showing subcellular heterogeneity within the malignant epithelial compartment.

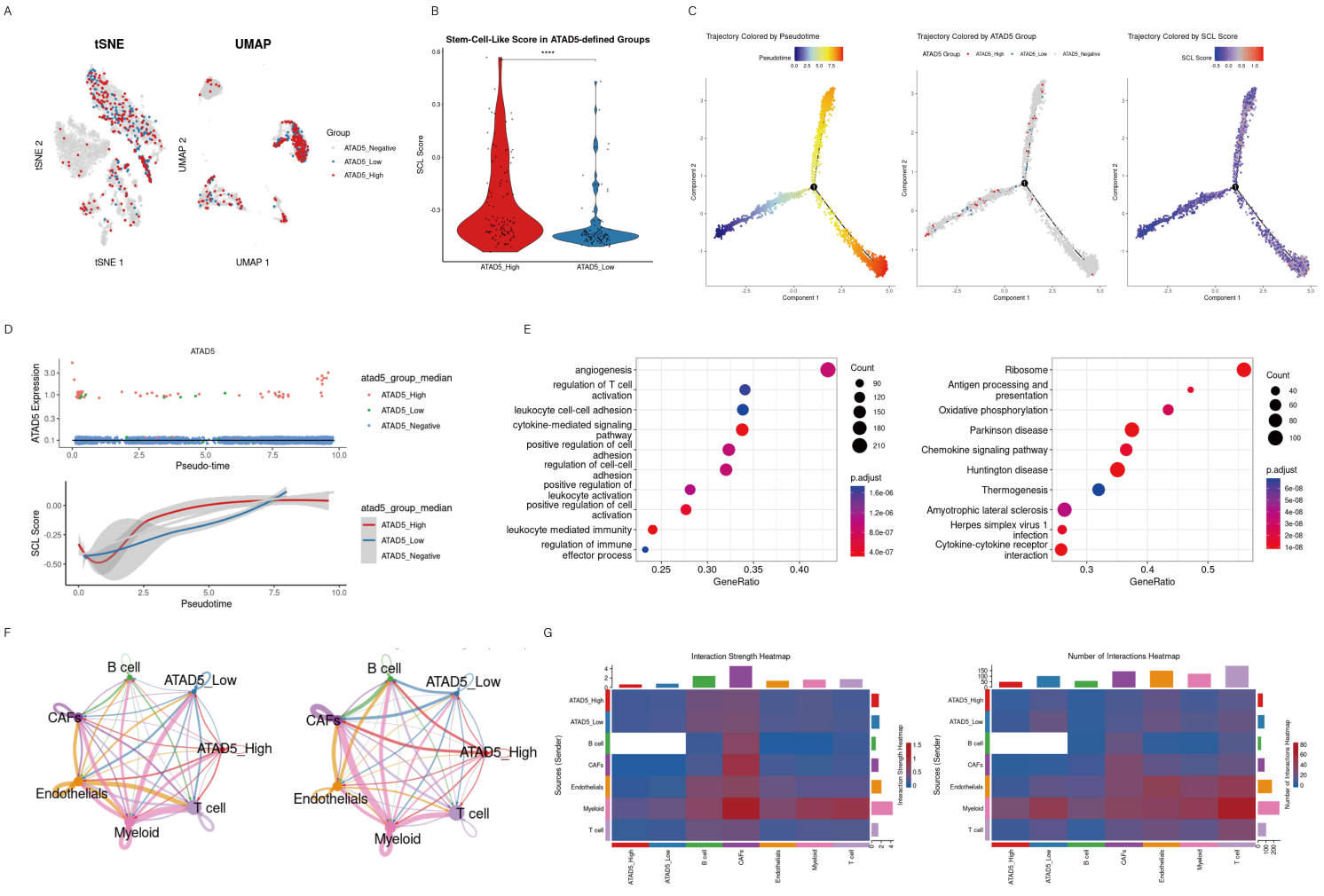


Figure 6

ATAD5-high malignant epithelial cells exhibit elevated stemness scores, distinct pseudotime trajectories, and active microenvironmental crosstalk. (A)tSNE and UMAP plots of malignant epithelial cells with ATAD5-high, ATAD5-low, and ATAD5-negative cells highlighted. (B)Violin plot showing significantly higher stemness-like (SCL) scores in ATAD5-high versus ATAD5-low malignant epithelial cells ($p < 0.0001$). (C)Pseudotime trajectory plots colored by pseudotime, ATAD5 group, and SCL score, showing enrichment of ATAD5-high cells at later pseudotime states with higher SCL scores. (D)Scatter plots of ATAD5 expression and SCL score along pseudotime for ATAD5-high, ATAD5-low, and ATAD5-negative groups. (E) Dot plots of GO and KEGG pathway enrichment in ATAD5-high malignant epithelial cells, highlighting angiogenesis, T cell activation regulation, leukocyte adhesion, and cytokine-mediated signaling. (F)CellChat chord diagrams showing predicted intercellular interaction networks among ATAD5-high, ATAD5-low, CAF, myeloid, T cell, B cell, and endothelial populations. (G)Heatmaps of predicted interaction strength and interaction number among cell populations, demonstrating stronger outgoing interactions from ATAD5-high cells toward CAFs and myeloid cells.

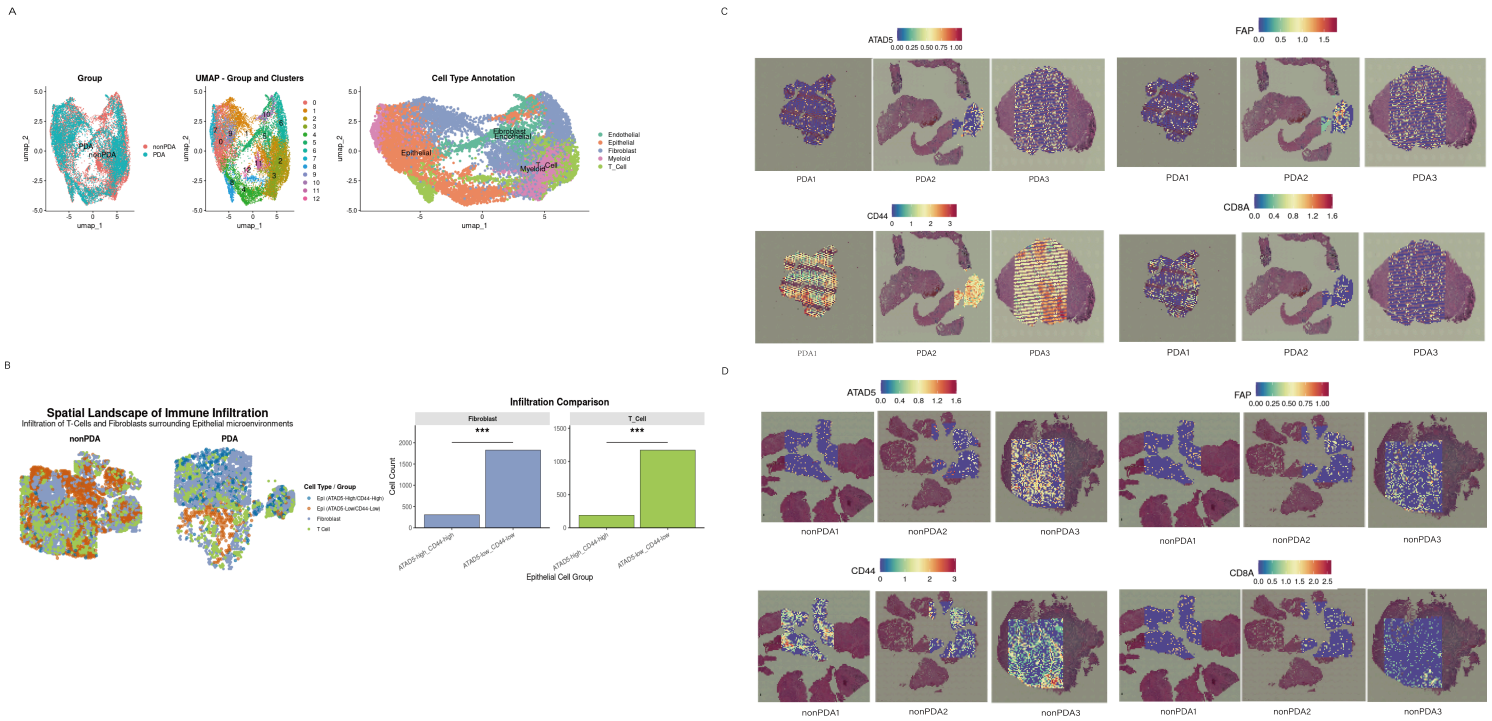


Figure 7

Spatial transcriptomics reveals co-enrichment of ATAD5 with stemness and stromal markers in prostatic ductal adenocarcinoma tissues. (A)UMAP plots of spatial transcriptomic data showing sample group distribution (PDA vs. non-PDA), cluster identities, and cell type annotation across six tissue sections. (B)Spatial landscape plots showing fibroblast and T cell infiltration patterns surrounding ATAD5-high and ATAD5-low epithelial microenvironments in PDA and non-PDA tissues, with quantification demonstrating significantly higher fibroblast and T cell counts adjacent to ATAD5-high/CD44-high epithelial spots ($p < 0.001$). (C)Spatial feature plots of ATAD5, FAP, CD44, and CD8A expression across three PDA tissue sections. (D) Spatial feature plots of ATAD5, FAP, CD44, and CD8A expression across three non-PDA tissue sections.

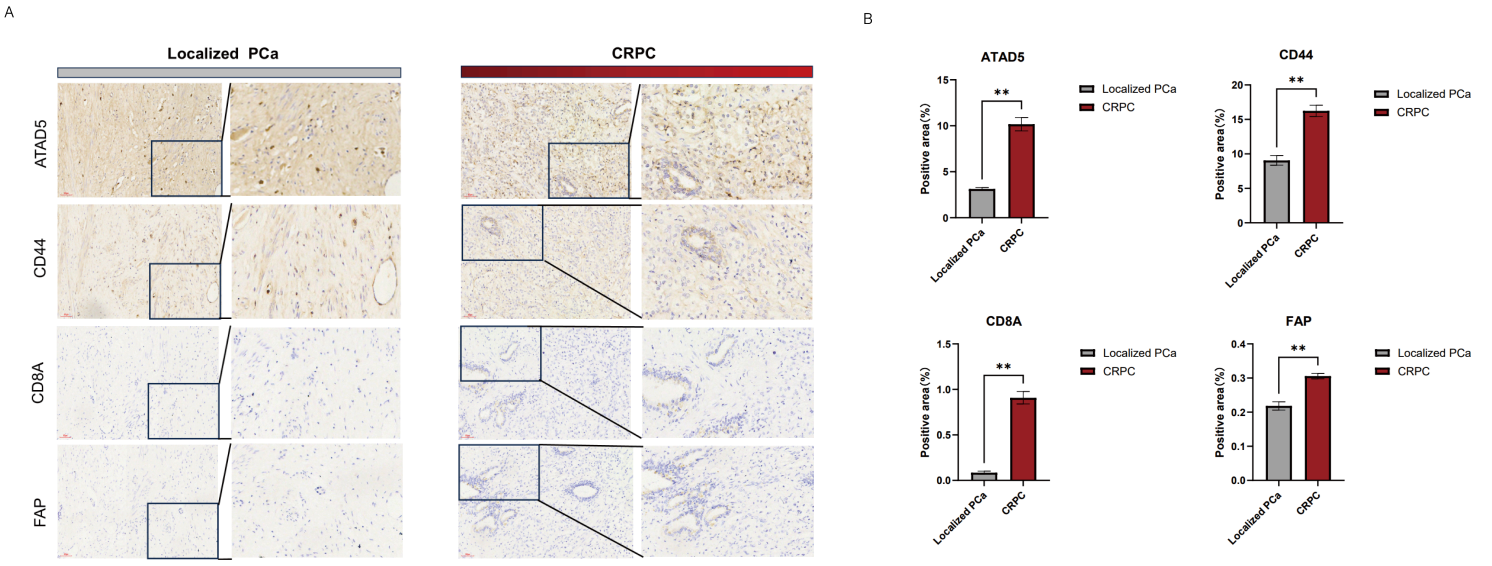


Figure 8

Immunohistochemistry confirms elevated ATAD5, CD44, CD8A, and FAP protein expression in CRPC clinical tissues. (A)Representative IHC images of ATAD5, CD44, CD8A, and FAP staining in localized prostate cancer (LPCa) and CRPC tissue sections. (B)Quantification of positive staining area (%) for ATAD5, CD44, CD8A, and FAP in LPCa (n = 10) and CRPC (n = 10) specimens; all four markers were significantly elevated in CRPC compared to LPCa (** p < 0.01, Mann–Whitney U test).

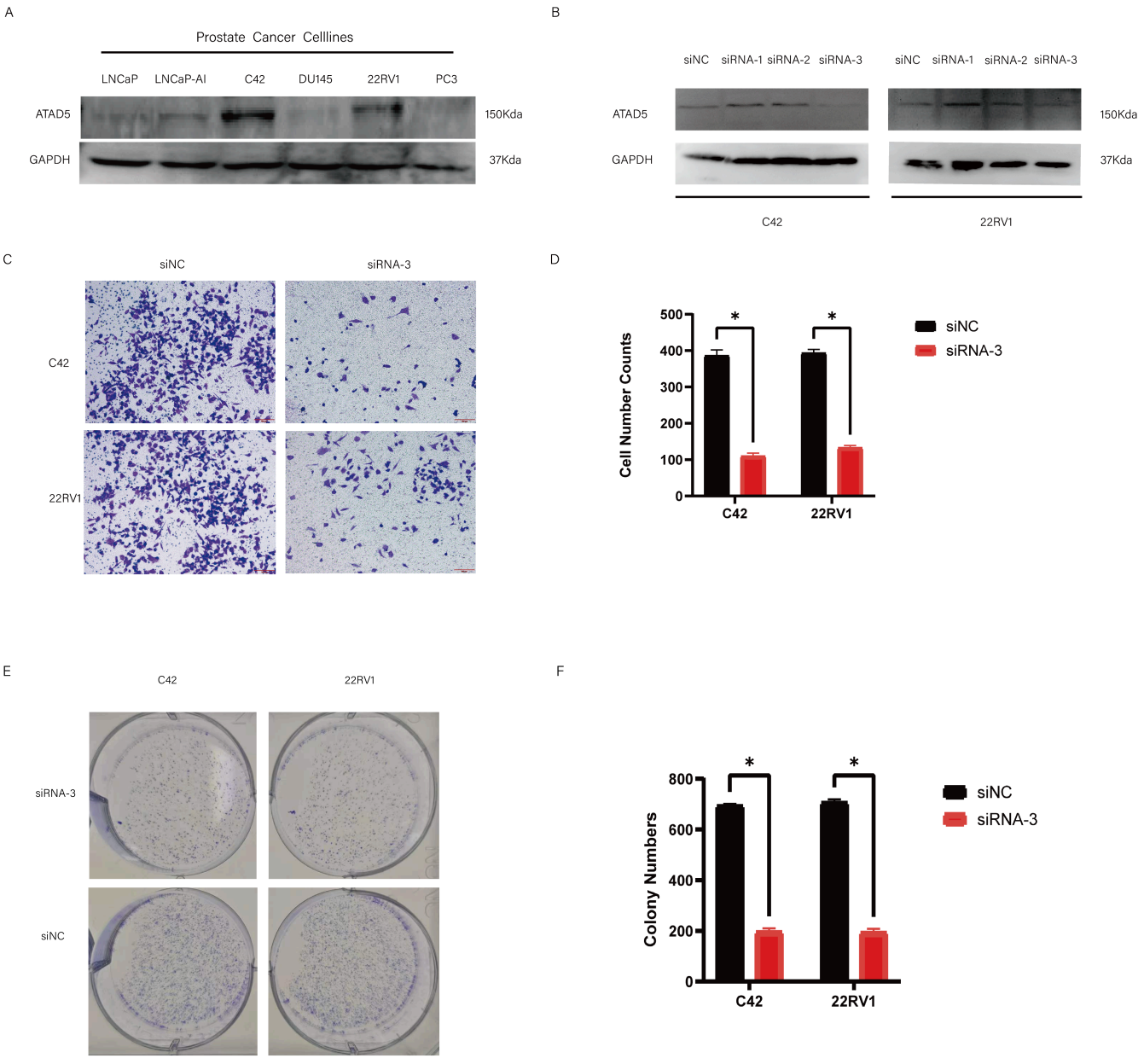


Figure 9

ATAD5 is highly expressed in CRPC cell lines and its depletion impairs invasion and colony formation. (A)Western blot showing ATAD5 protein expression across six prostate cancer cell lines (LNCaP, LNCaP-AI, C4-2, DU145, 22Rv1, PC3); GAPDH served as loading control. (B)Western blot confirming ATAD5 knockdown efficiency by siRNA-1, siRNA-2, and siRNA-3 in C4-2 and 22Rv1 cells relative to siNC control. (C)Representative Transwell images showing reduced cell invasion in siRNA-3-transfected C4-2 and 22Rv1 cells compared to siNC. (D)Quantification of invaded cell numbers; ATAD5 knockdown significantly reduced invasion in both cell lines (* $p < 0.05$). (E)Representative colony formation images showing reduced colony numbers in siRNA-3-transfected C4-2 and 22Rv1 cells. (F)Quantification of colony numbers; ATAD5 knockdown significantly reduced clonogenic capacity in both cell lines (* $p < 0.05$).